Nanoscale Advances

ROYAL SOCIETY OF CHEMISTRY

COMMUNICATION

View Article Online
View Journal | View Issue

Cite this: *Nanoscale Adv.*, 2026, **8**, 1191

Received 8th September 2025
Accepted 24th December 2025

DOI: 10.1039/d5na00862j

rsc.li/nanoscale-advances

Effect of single xeno-nucleic acid replacement on the fluorescence of DNA-encapsulated silver nanoclusters

Hari Chandana Yadavalli,†[af] Riddhi Nagda,†[ae] Jooyoun Kang,[b] Minhaeng Cho,[bc] Chenguang Lou,[d] Seong Wook Yang,*[a] Peter Waaben Thulstrup,*[e] Morten Jannik Bjerrum*[e] and Pratik Shah*[f]

The fluorescent properties of DNA/AgNCs are largely governed by the composition of AgNCs, the nucleobase sequence, and the secondary structure of the DNA template. Here, by systematic incorporation of xeno-nucleic acid modifications, we demonstrate the potential of altering the sugar chemistry of the template DNA backbone, as a novel factor in AgNC fluorescence modulation.

DNA-encapsulated silver nanoclusters (DNA/AgNCs) have emerged as versatile fluorescent probes, offering bright visible-to-NIR emission, large Stokes shifts, and significant promise for bioimaging and biosensing applications.[1–5] A consistent effort has been made to investigate the effects of sequence, secondary structure, and synthesis conditions on tuning the fluorescence emission of DNA/AgNCs.[3,6–8] Efforts to synthesize DNA/AgNCs almost exclusively take advantage of natural nucleic acid chemistry that involves using mostly DNA and, in a few cases, RNA templates.[9]

Ag^+ has a higher affinity for cytosines due to the presence of nitrogen atoms that are available for coordination with Ag ions.[10,11] Screening DNA sequences rich in 2′-deoxycytidine, or occasionally 2′-deoxyguanosine, remains central to tuning AgNC emission, though the use of unnatural nucleic acid chemistries in their synthesis is still scarcely explored. Cerretani *et al.* have used an inosine base in DNA, while Weadick and Liu have used phosphorothioate modification in DNA.[12,13] However, sugar backbone modifications remain underexplored for their effects on the photophysical properties of AgNCs. Nucleoside modifications have emerged as key tools for tuning nucleic acids, with Xeno-Nucleic Acids (XNAs) featuring altered sugar backbones mainly influencing stability, functionality, and DNA conformations (A/B/Z forms).[14–16] Various XNAs have been developed so far,[17] where Locked Nucleic Acid (LNA) and Arabinonucleic Acid (ANA) (Fig. 1A and Scheme S1) are two examples. Both LNA and ANA have been used extensively in nucleic acid technologies to substitute natural nucleosides with LNA and ANA offers enhanced binding stability and structural flexibility for enzymatic activity, respectively.[18,19]

Recent studies have demonstrated the mutual influence of the DNA secondary structure and AgNCs on each other.[20] For example, AgNCs mediated the non-canonical head-to-head dimerization of hairpin and triplex DNAs, which influences the fluorescence emission of DNA/AgNCs.[20,21] One of the contributors to the DNA secondary structure is the backbone sugar. Therefore, in this study, we aimed to investigate the effect of backbone sugar conformations on the photophysical properties of AgNCs encapsulated in hairpin DNAs.

The hairpin-loop DNA structure used is known to form head-to-head dimerization mediated by AgNCs. We used an oligodeoxynucleotide 9A-7C-30T (referred to as DNA), which includes a 7-mer 2′-deoxycytidine (7dC) loop (Table S1). We first identified key residues in the 2′-deoxycytidine loop and used these structural insights to systematically replace the deoxyribose of the key cytidine residues with XNAs.[22]

The DNA-encapsulated AgNCs exhibited mainly three different emission patterns: orange (Ex/Em: 480/590 nm), red (Ex/Em: 560/640 nm), and far-red (Ex/Em: 660/730 nm), with orange being the most prominent emitter (Fig. 1B). Adenine and thymine in the DNA hairpin stem region are expected to ensure that the key AgNC interaction sites are located within the 7dC hairpin. We confirmed that the DNA/AgNCs generated a non-canonical head-to-head dimer structure mediated by orange emissive AgNCs using native gel electrophoresis, while no detectable red or far-red emission could be observed on the gel (Fig. S1). Herein, we performed a comparative study between the DNA/AgNCs enclosed in

[a]*Department of Systems Biology, Institute of Life Science and Biotechnology, Yonsei University, Seoul, 03722, Korea. E-mail: yang@yonsei.ac.kr*

[b]*Center for Molecular Spectroscopy and Dynamics, Institute for Basic Science, Seoul 02841, Korea*

[c]*Department of Chemistry, Korea University, Seoul 02841, Republic of Korea*

[d]*Department of Physics, Chemistry, and Pharmacy, University of Southern Denmark, Campusvej 55, 5230 Odense M, Denmark*

[e]*Department of Chemistry, University of Copenhagen, Copenhagen 2100, Denmark. E-mail: mobj@chem.ku.dk; pwt@chem.ku.dk*

[f]*Department of Science and Environment, Roskilde University, Roskilde 4000, Denmark. E-mail: shah@ruc.dk*

† These authors contributed equally to this work.

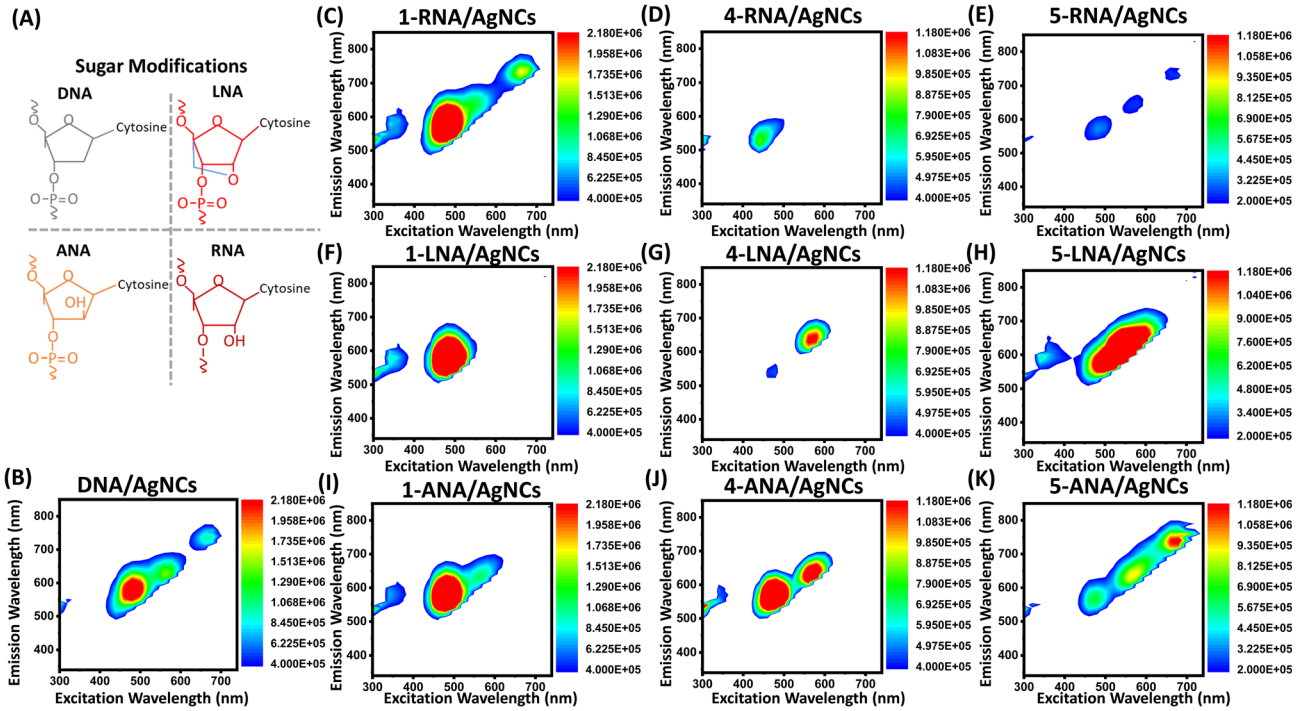

Fig. 1 Tuning fluorescence emission based on sugar modification. (A) Chemical structures of the sugars replaced in the DNA backbone. (B–J) Fluorescence spectra of XNA/AgNCs encapsulated by the corresponding DNA (B), RNA (C–E), LNA (F–H) or ANA (I–K) templates modified at the 1st, 4th and 5th positions of their respective sugar backbones. Samples were excited for every 10 nm from 320 nm to 720 nm.

both the DNA templates (9A-6C-30T and 9A-7C-30T). 9A-6C-30T/AgNCs only exhibited bright orange (Ex/Em: 480/590 nm) fluorescence, and no red or far-red emissions were observed (Fig. S1A). Following this, we performed an in-gel fluorescence assay comparing 9A-6C-30T/AgNCs and DNA/AgNCs. The dimerized DNA structure encapsulating orange emissive AgNCs can be observed on the gel when excited under UV illumination (Fig. S1C). Furthermore, red emissive AgNCs were either found to be encapsulated in a smaller hairpin DNA structure, as shown when using DNA 6C-miR-159-8bp, or in a green emissive dimerized structure of 10A-10T-7C-10T DNA (Fig. S2). Both results are consistent with our previous reports discussing these phenomena.[20,21,23] We also compared the DNA (9A-7C-30T) to an unstructured primer (46 nucleotides in length). On the gel, a hairpin structure forming DNA (9A-7C-30T) runs slightly faster than the 46nt. linear DNA of a similar size (Fig. S3). DNA shows two bands: a faint linear DNA that runs slower than the 20bp size marker and at a length similar to 46nt linear unstructured DNA and a slightly faster running hairpin structure. Furthermore, non-hairpin structure-forming DNAs 7C-9A-miR21-22bp and 7C-30T-miR21-22bp (Fig. S4) do not encapsulate any orange-emissive AgNCs, while Watson-Crick base-paired duplex DNA/AgNCs 7C-9A-miR-21-22bp and 7C-30T-miR-21-22bp templates exhibited distinct fluorescence, confirming that AgNC fluorescence was not formed by duplex DNA (Fig. S4A–E). Compared to the various control DNAs discussed above, the orange-emissive DNA/AgNCs runs significantly slower and is therefore considered the dimerized DNA.

Next, we varied the local backbone sugar of one 2′-deoxycytidine (dC, South-type) to cytidine (rC, North-type) along the 7dC loop in a systematic manner. Here, nomenclature denotes the substituted cytidine's position from the 5′ end of the 7dC loop and the XNA sugar type; for instance, 1-RNA indicates replacing the first 5′ end dC with rC in the 7dC hairpin. When substituting ribose sugar for deoxyribose sugar, we observed that the fluorescence characteristics of encapsulated AgNCs were only slightly affected compared to those of DNA/AgNCs in most cases (Fig. 1C). However, the fluorescence was noticeably reduced (>20-fold) for 4-RNA/AgNCs and 5-RNA/AgNCs compared to DNA/AgNCs (Fig. 1D and E). We confirmed using gel electrophoresis that the diminishing fluorescence of 4-RNA/AgNCs and 5-RNA/AgNCs correlated with the inability of oligos to mediate head-to-head dimerization (Fig. S5E and F and S6, lanes 9–12). These results indicate that the fourth and fifth cytidines of the 7dC-loop play a crucial role in the formation of the head-to-head hairpin DNA dimer directed by the sugar chemistry of the backbone. Due to the steric and gauche effects, the pentose rings of DNA, RNA/LNA, and ANA are known to adopt the South (3′-*endo*), North (2′-*endo*) and near-East/East (O4′-*endo*) conformations, respectively.[22,24] We also reported that the local pentose conformation changes induced by RNA incorporation could tune the fluorescence of AgNCs.[20] This is likely due to the presence of the 2′-OH group at the pentose ring in RNA, which is absent in DNA (Fig. 1A). Therefore, we hypothesized that actuating the pentose ring to adopt other conformations (such as North-type and East-type) could further modulate the emission properties of AgNCs.

Therefore, in addition to RNA substitutions, we tested the same hairpin sequence *via* LNA and ANA modifications. In LNA, the pentose ring is "locked" into a North-type conformation (3′-*endo*)

by a methylene bridge between the 2′ oxygen and 4′ carbon atoms.[22,25] In ANA, the canonical ribofuranose sugar of DNA/RNA is replaced by the arabinose sugar, which causes the pentose ring to adopt near-East/East (O4′-*endo*) conformations.[22,24] We hypothesized that incorporating RNA, ANA, or LNA into the 7dC loop alters local sugar conformations and thus AgNC fluorescence; systematic LNA-C substitutions across the loop revealed prominent fluorescence changes with backbone modification. Compared to DNA/AgNCs, 1-LNA/AgNCs showed increased orange fluorescence with (Ex/Em: 480/590 nm) and a significant reduction in the red and far-red emissions (Fig. 1F). A similar absence of far-red emission was also observed for all the LNA modifications (Fig. S7). This is probably due to the two different sugar conformations between dC (South-type) and LNA-C (North-type). In comparison to 1-LNA/AgNCs, both 2-LNA/AgNCs and 7-LNA/AgNCs exhibited reduced red emissions. Furthermore, the fluorescence spectra of 4-LNA/AgNCs and 5-LNA/AgNCs were significantly changed (Fig. 1G and H). The results revealed a clear positioning effect of LNA-C substitution on the fluorescence of DNA/AgNCs. In contrast to 4-RNA/AgNCs and 5-RNA/AgNCs, neither 4-LNA/AgNCs nor 5-LNA/AgNCs shows diminished fluorescence; rather, the emission maxima were red-shifted. While the orange emission, with an Ex/Em: 480/590 nm, from 4-LNA/AgNCs was significantly reduced (>90%), it retained red-emissive AgNCs (Ex/Em: 560/640 nm). Such a difference may be caused by the more rigid sugar conformation of LNA-C when compared to rC. Not surprisingly, 5-LNA/AgNCs generated fluorescence with Ex/Em: 540/620 nm, which is distinct compared to DNA/AgNCs or other LNA/AgNCs (Fig. 1 and S7). The results confirmed our initial hypothesis: different backbone sugar chemistry could significantly influence the fluorescent properties of AgNCs. It is important to note that commercially available LNA-C modifications are methylated at Carbon-5 of the cytosine base. To rule out methylated cytosine influence in LNA, we synthesized AgNCs using 5-methylcytosine at positions 2, 4, and 7 of the 7dC-loop, confirming emission spectra distinct from LNA-modified AgNCs and highlighting the unique influence of backbone sugar chemistry on emission (Fig. S8A–C).

We next used ANA-incorporated DNA/AgNCs (ANA/AgNCs). ANA-C has D-arabinose sugar in the backbone, which is reported to adopt near-East/East conformations (4O′-*endo*).[22,24] Of note, the cytosine base is not methylated in the commercially available ANA-C-modified oligonucleotides. ANA-C-incorporated DNA/AgNCs showed distinct fluorescent properties compared to DNA/AgNCs, RNA/AgNCs, and LNA/AgNCs. We ascribed the different fluorescent properties to the near-East/East conformations of ANA-C. For example, 1-ANA, 3-ANA, and 4-ANA encapsulated AgNCs exhibited orange emission with Ex/Em: 480/590 nm and retained minor red-emissive AgNCs (Ex/Em: 560/640 nm) (Fig. 1I–K). However, 2-ANA and 5-ANA encapsulated AgNCs retained emission in the far-red spectrum with Ex/Em at 660/740 nm but with a significant reduction (>4-fold) in both orange and red emissions. Both 6-ANA/AgNCs and 7-ANA/AgNCs showed significantly reduced orange emission, with 6-ANA/AgNCs exhibiting red fluorescence with Ex/Em at 560/640 nm (Fig. 2 and S9). While both 4-RNA/AgNCs and 4-LNA/AgNCs exhibited significantly reduced orange emissions, 4-ANA/AgNCs maintained high orange and red emissions. Similarly, while 5-RNA/AgNCs generated reduced orange emissions and 5-LNA/AgNCs with distinct, red-shifted fluorescence (Ex/Em: 540/620 nm) compared to DNA/AgNCs, 5-ANA/AgNCs generated far-red emissions as the major fluorescence with significantly reduced red and orange emissions (Fig. 1 and S9). This likely results from the different backbone sugar conformations between ANA and LNA/RNA.[22] Taking the results together, our data indicate that the backbone sugar chemistry has a significant impact on the fluorescent properties of AgNCs, especially at positions 4 and 5 of the cytosine loop, which are involved in the formation of a non-canonical head-to-head dimer DNA structure mediated by AgNCs.

Previous reports determined that the orange fluorescence was due to the formation of a non-canonical head-to-head dimer structure, which is a result of the cytosines of the 7dC loop flipping out to form head-to-head dimerized DNA/AgNCs.[20] We also checked the presence of other possible secondary structures of XNA/AgNCs using gel electrophoresis. Using SYBR Gold staining, we found that RNA-, LNA-, and ANA-modified nucleic acids encapsulating AgNCs formed an orange-emissive DNA/AgNC head-to-head dimer, along with smaller SYBR-stained structures (hairpin and linear ssDNA) that did not encapsulate detectable AgNCs (Fig. 2, lanes 1 and 2). The gel electrophoresis has limited success in visualizing red or far-red AgNCs, as red-emissive AgNCs either lose fluorescence or transform into green-emissive AgNCs in response to oxidation, while far-red AgNCs are less excitable using a UV light source.[21] This phenomenon was also observed with the structural analysis of AgNCs encapsulated in the hairpin structure forming 6C-miR-159-8bp and the triplex structure forming 10A-10T-7C-10T (Fig. S2). All the LNA/AgNC and ANA/AgNC modifications showed similar DNA/AgNC secondary structures when looking at the SYBR gold-stained DNA/AgNC bands, regardless of the positions at which LNAs or ANAs were incorporated. Interestingly, 3-LNA/AgNCs showed red-emissive AgNC fluorescence in a smaller, likely hairpin DNA/AgNC structure, which is consistent with our previous

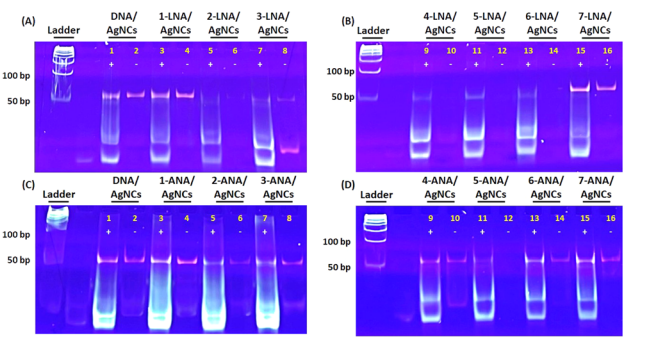

Fig. 2 Native PAGE in-gel fluorescence assay of XNA/AgNCs. (A–D) Structural analysis of DNA (A and C) *vs.* LNA (A and B) and ANA (C and D). Samples were visualized with AgNCs and either with (+) or without (–) SYBR Gold DNA staining (+) or AgNCs (–). A GeneRuler 50 bp DNA ladder was used as the size marker, with the lowest band corresponding to 50 bp. The ladder was stained using SYBR Gold DNA staining solution.

report.[23] This is consistent with fluorescence data, whereby 3-LNA/AgNCs shows nearly 2-fold higher red emission compared to the DNA/AgNC control (Fig. 2A, lanes 7 and 8). 4-LNA/AgNCs did not show any head-to-head dimer DNA structure consistent with the drop in fluorescence emission (Fig. 2A and B, lanes 9 and 10). This differential stability of orange emissive AgNCs can explain the absence of detectable 5-LNA/AgNCs or 6-LNA/AgNCs on gel. ANA incorporated DNA/AgNCs mostly showed a non-canonical head-to-head dimer DNA structure, with 4-ANA/AgNCs exhibiting faint red emission. 5-ANA/AgNCs could not be detected, likely due to the far-red emissive AgNCs, which cannot be visualized in gel using UV excitation (Fig. 2C and D). However, no significant difference in the secondary structures of DNA was observed when stained using SYBR Gold dye. Previously, we have reported a comparative study about the differential stability of DNA/AgNC post-synthesis.[26] While orange emissive DNA/AgNCs retain their fluorescence for up to 3 weeks, the red emissive DNA/AgNCs encapsulated in hairpin DNA are oxidized in less than 48 hours due to oxidation. The red emission recovered upon adding the reducing agent.[21] Therefore, we evaluated AgNC fluorescence stability post-synthesis. The red emission of AgNCs encapsulated within LNA and DNA templates was reduced by more than 80%, likely due to oxidation (Fig. S10). Based on these data, we observed that although the 2-, 5-, and 6-LNA/AgNCs showed red emission initially, the 3-LNA/AgNCs retained the strongest red fluorescence for up to 6 hours (Fig. S10A). This explains the red hairpin band observed in the in-gel fluorescence assay (Fig. 2), which was not seen in the other modifications. Based on the above data, we suggest that orange emissive AgNCs are less affected by oxidation when compared with red-emissive DNA/AgNCs. However, interestingly, the orange emissive AgNCs exhibited differential stability depending on the sugar backbone of the template. While DNA, 1-LNA, and 7-LNA encapsulated AgNCs retained >90% orange emission, other LNA/AgNCs (2-, 3-, 5-, and 6-LNA/AgNCs) lost significant (nearly 80%) orange emission within 6 hours. Overall, the results suggest that almost all the XNA incorporated DNA/AgNCs generated comparatively similar secondary structures, and therefore, the differences in fluorescence spectra likely result from the distinct local backbone sugar conformations of the three XNA modifications. We used far-UV, circular dichroism (CD) to assess if the local XNA modifications could induce any major structural changes of the hairpin DNA. We show the CD data for DNA and the 2-, 5-XNA variants. These data show some minor variations, but overall, the CD signatures are similar, with a minimum below 250 nm and a maximum above 275 nm before AgNC formation (Fig. S11). The CD after this reaction is significantly altered for the reaction mixtures with a significant drop in intensity, in particular for the positive CD band, and with non-zero ellipticity extending above 350 nm (Fig. S11). The UV-Vis absorbance characteristics of the reaction mixtures for DNA sequences with XNA at positions 2 and 5 show considerable variation, but all exhibit several absorbance features throughout the visible and into the near infrared region (Fig. S12).

Next, we wanted to investigate if the XNA incorporation affected the fluorescence lifetime, which can be affected by the changes in the local environment, including rigidity. Therefore, using time-correlated single-photon counting, we measured the time-resolved fluorescence of DNA/AgNCs with and without XNA incorporation. A bi-exponential model was globally applied to fit the fluorescence decay curves satisfactorily.[20] The average decay time of orange-emissive DNA/AgNCs was found to be 2.49 ns derived from two species with decay times of 0.20 ns and 4.01 ns, with a major contribution to the observed fluorescence originating from the component with a decay time of 4.01 ns (Fig. S13 and Table S2). Even with the RNA, LNA, or ANA incorporations, the average decay time was found to vary between 2.96 ns and 4.53 ns.

Next, we wanted to evaluate whether the altered photophysical properties in XNA/AgNCs are the result of the altered AgNC composition compared to DNA/AgNCs using ESI-mass spectrometry. It is important to acknowledge that the AgNCs will fragment during the process.[27] In DNA/AgNCs, four distinct nanoclusters were observed, incorporating 6, 9, 13, and 14 silver atoms (Tables S3 and S4). When the 2′-deoxyribose was replaced with RNA, LNA, and ANA sugars, some differences in the AgNC composition across templates were observed. The AgNC composition remained largely unchanged when modifications were introduced at 2-cytosine. The main difference was found for 2-RNA/AgNCs that exhibited a broader range of AgNC species and were missing the cluster with 14 silver atoms (Table S4), suggesting a somewhat changed binding site. However, there were distinct differences when modifications were introduced at the 5-cytosine position. 5-RNA and 5-LNA encapsulated AgNCs displayed only Ag_{13} as the predominant AgNC species. 5-LNA/AgNCs and 5-RNA/AgNCs contained 13 silver atoms, while 5-ANA/AgNCs exhibited AgNCs with 6, 9, and 13 Ag atoms. In the ESI-MS data for 2-LNA and 2-ANA, the most abundant charge states correspond to Ag_{13} and Ag_{14}, with $N_0 = 6$, which corresponds to red emission.[28–30] These closed-shell electron configurations are reported to yield orange to red or far-red fluorescence.[28–30] Thus, our ESI-MS data align with the previously observed fluorescence species, determining the orange to red fluorescence range dominated by the $N_0 = 6$ or 8 atomic species.[28–30] The results again confirmed that different local backbone sugar conformations, due to the introduction of XNAs, likely altered the composition of AgNCs and thereby modulated the emission properties of AgNCs. This reveals, for the first time, a crucial role of the local sugar conformation of the 7dC-loop backbone in the outward base flipping, which in turn forms non-canonical head-to-head dimerized DNA/AgNCs.

Conclusions

In this study, we investigated how different backbone sugar conformations could influence the fluorescence of DNA/AgNCs and the structure of DNA/AgNCs. Our findings demonstrate that XNA modifications, such as the substitution of the 2′-deoxyribose of cytidine with the LNA, ANA, or RNA sugars at different positions within the 7dC-loop, revealed distinct impacts on the

fluorescence emission and the structural integrity of the DNA/AgNCs. We ascribe these changes to the local backbone sugar conformations due to the XNA incorporation. Our study underscores the importance of sugar backbone modifications in tuning the fluorescence and structural properties of DNA/AgNCs. The novel insights and potential use of XNA expand the chemical space that can be explored for the rational design of DNA/AgNCs for applications in biosensing, bioimaging, and DNA nanotechnology.

Author contributions

H. C. Yadavalli: writing – original draft, investigation, and analysis. H. C. Yadavalli, R. Nagda: analysis, investigation, data curation, and validation. M. J. Bjerrum and P. W. Thulstrup: original draft, investigation, and analysis. J. Kang, M. Cho, and C. Lou: writing – review & editing. S. W. Yang: writing – review & editing, supervision, methodology, and funding acquisition. P. Shah: conceptualization, writing – review & editing, supervision, project administration, resources, methodology, and funding acquisition.

Conflicts of interest

There are no conflicts to declare.

Data availability

The data supporting this article have been included as part of the supplementary information (SI). Supplementary information: Tables S1 with oligo sequence, fluorescence and CD spectra, ESI-MS and gel electrophoresis data and further experimental details. See DOI: https://doi.org/10.1039/d5na00862j.

Acknowledgements

P. Shah acknowledges funding from the Novo Nordisk Foundation (NNF23OC0086984). S. W. Yang acknowledges funding from the National Research Foundation of Korea (NRF), funded by the Ministry of Science, ICT, and Future Planning (RS-2023-NR077248); the Basic Science Research Program (RS-2018-NR031069); and the Korea Health Technology R&D Project through the Korean Healthy Industry Development Institute (KHIDI), funded by the Ministry of Health & Welfare (RS-2021-KH112367).

Notes and references

1 J. T. Petty, J. Zheng, N. V. Hud and R. M. Dickson, *J. Am. Chem. Soc.*, 2004, **126**, 5207–5212.
2 P. Mastracco, A. Gonzàlez-Rosell, J. Evans, P. Bogdanov and S. M. Copp, *ACS Nano*, 2022, **16**, 16322–16331.
3 M. Yang, X. Chen, Y. Su, H. Liu, H. Zhang, X. Li and W. Xu, *Front. Chem.*, 2020, **8**, 601621.
4 L. Rolband, L. Yourston, M. Chandler, D. Beasock, L. Danai, S. Kozlov, N. Marshall, O. Shevchenko, A. V. Krasnoslobodtsev and K. A. Afonin, *Molecules*, 2021, **26**, 4045.
5 L. Danai, L. A. Rolband, V. A. Perdomo, E. Skelly, T. Kim and K. A. Afonin, *Nanomedicine*, 2023, **18**, 769–782.
6 P. Shah, S. K. Cho, P. W. Thulstrup, Y.-J. Bhang, J. C. Ahn, S. W. Choi, A. Rørvig-Lund and S. W. Yang, *Nanotechnology*, 2014, **25**, 045101.
7 L. E. Yourston, A. Y. Lushnikov, O. A. Shevchenko, K. A. Afonin and A. V. Krasnoslobodtsev, *Nanomaterials*, 2019, **9**, 613.
8 M. Chandler, O. Shevchenko, J. L. Vivero-Escoto, C. D. Striplin and K. A. Afonin, *J. Chem. Educ.*, 2020, **97**, 1992–1996.
9 P. Shah, P. W. Thulstrup, S. K. Cho, M. J. Bjerrum and S. W. Yang, *Chem. Commun.*, 2014, **50**, 13592–13595.
10 C. M. Ritchie, K. R. Johnsen, J. R. Kiser, Y. Antoku, R. M. Dickson and J. T. Petty, *J. Phys. Chem. C*, 2007, **111**, 175–181.
11 A. Ono, S. Cao, H. Togashi, M. Tashiro, T. Fujimoto, T. Machinami, S. Oda, Y. Miyake, I. Okamoto and Y. Tanaka, *Chem. Commun.*, 2008, 4825–4827.
12 C. Cerretani, M. B. Liisberg, V. Rück, J. Kondo and T. Vosch, *Nanoscale Adv.*, 2022, **4**, 3212–3217.
13 D. S. Weadick and J. Liu, *Nanomaterials*, 2015, **5**, 804–813.
14 N. Martín-Pintado, M. Yahyaee-Anzahaee, R. Campos-Olivas, A. M. Noronha, C. J. Wilds, M. J. Damha and C. Gonzalez, *Nucleic Acids Res.*, 2012, **40**, 9329–9339.
15 I. Anosova, E. A. Kowal, M. R. Dunn, J. C. Chaput, W. D. Van Horn and M. Egli, *Nucleic Acids Res.*, 2015, **44**, 1007–1021.
16 L. K. McKenzie, R. El-Khoury, J. D. Thorpe, M. J. Damha and M. Hollenstein, *Chem. Soc. Rev.*, 2021, **50**, 5126–5164.
17 D. Novikova, A. Sagaidak, S. Vorona and V. Tribulovich, *Molecules*, 2024, **29**, 3025.
18 Y. V. Pabon-Martinez, Y. Xu, A. Villa, K. E. Lundin, S. Geny, C.-H. Nguyen, E. B. Pedersen, P. T. Jørgensen, J. Wengel, L. Nilsson, C. I. E. Smith and R. Zain, *Sci. Rep.*, 2017, **7**, 11043.
19 A. A. Williams, A. Darwanto, J. A. Theruvathu, A. Burdzy, J. W. Neidigh and L. C. Sowers, *Biochemistry*, 2009, **48**, 11994–12004.
20 P. Shah, R. Nagda, I. L. Jung, Y. J. Bhang, S.-W. Jeon, C. S. Lee, C. Do, K. Nam, Y. M. Kim, S. Park, Y. H. Roh, P. W. Thulstrup, M. J. Bjerrum, T.-H. Kim and S. W. Yang, *ACS Nano*, 2020, **14**, 8697–8706.
21 R. Nagda, S. Park, I. L. Jung, K. Nam, H. C. Yadavalli, Y. M. Kim, K. Yang, J. Kang, P. W. Thulstrup, M. J. Bjerrum, M. Cho, T.-H. Kim, Y. H. Roh, P. Shah and S. W. Yang, *ACS Nano*, 2022, **16**, 13211–13222.
22 M. Egli, in *The Excitement of Discovery: Selected Papers of Alexander Rich: A Tribute to Alexander Rich*, World Scientific, 2019, pp. 309–315.
23 P. Shah, S. W. Choi, R. Nagda, R. Geczy, S. K. Cho, Y. J. Bhang, T.-H. Kim, T. Y. Song, P. H. Lee, J.-H. Kang, P. W. Thulstrup, M. J. Bjerrum, I. L. Jung and S. W. Yang, *Nanoscale*, 2018, **10**, 20717–20722.

24 A. Y. Denisov, A. M. Noronha, C. J. Wilds, J.-F. Trempe, R. T. Pon, K. Gehring and M. J. Damha, *Nucleic Acids Res.*, 2001, **29**, 4284–4293.
25 M. Petersen, K. Bondensgaard, J. Wengel and J. P. Jacobsen, *J. Am. Chem. Soc.*, 2002, **124**, 5974–5982.
26 R. Nagda, P. Shah, C. S. Lee, S. Park and S. W. Yang, *Nanomaterials*, 2019, **9**, 667.
27 R. Guha, S. Malola, M. Rafik, M. Khatun, A. Gonzàlez-Rosell, H. Häkkinen and S. M. Copp, *Nanoscale*, 2024, **16**, 20596–20607.
28 S. M. Copp, D. Schultz, S. Swasey, J. Pavlovich, M. Debord, A. Chiu, K. Olsson and E. Gwinn, *J. Phys. Chem. Lett.*, 2014, **5**, 959–963.
29 A. Hajda, R. Guha, S. M. Copp and J. Olesiak-Bańska, *Chem. Sci.*, 2025, **16**, 1737–1745.
30 A. Gonzàlez-Rosell and S. M. Copp, *Acc. Chem. Res.*, 2024, **57**, 2117–2129.